analytical chemistry

Article

pubs.acs.org/ac

Concentration Measurement of Length-Fractionated Colloidal Single-Wall Carbon Nanotubes

Constantine Y. Khripin,[†] Xiaomin Tu,[†] John Howarter,[†,‡,§] Jeffrey Fagan,[†] and Ming Zheng*,[†]

[†]Polymers Division, National Institute of Standards and Technology, 100 Bureau Drive, Gaithersburg, Maryland 20899-8542, United States

[‡]School of Materials Engineering, and [§]Division of Environmental and Ecological Engineering, Purdue University, West Lafayette, Indiana 47907, United States

Supporting Information

ABSTRACT: The determination of the carbon concentration of single-wall carbon nanotubes (SWCNTs) in a given dispersion is a basic requirement for many studies. The commonly used optical absorption-based concentration measurement is complicated by the spectral change due to variations in nanotube chirality and length. In particular, the origin of the observed length-dependent spectral change and its effect on concentration determination has been the subject of considerable debate. Here, we use length-fractionated DNA-wrapped SWCNTs to establish the relationship between SWCNT carbon concentration and optical absorption spectra by directly quantifying the amount of wrapping DNA and, independently, the DNA/carbon nanotube mass ratio. We find that SWCNT carbon concentrations derived from either the E_{11} peak or spectral baseline deviate significantly from the SWCNT carbon concentrations derived from the DNA measurement method. Instead, SWCNT carbon concentrations derived from the spectral integration of the E_{11} optical transition region match most closely with the DNA-derived SWCNT carbon concentrations. We also observe that shorter SWCNT fractions contain more curved carbon nanotubes, and propose that these defective nanotubes are largely responsible for the observed spectral variation with nanotube length.

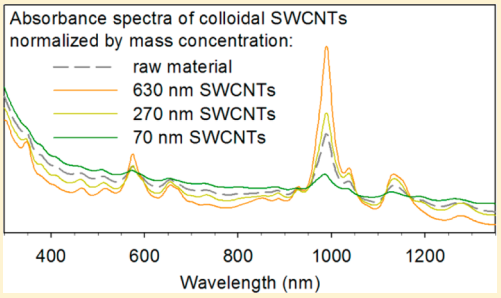

Single-wall carbon nanotubes (SWCNTs) are hydrophobic allotropes of carbon, normally insoluble in water. SWCNTs can be made water-soluble by dispersion with small-molecule surfactants and macromolecules,[1−7] enabling fundamental studies of colloidal SWCNTs. For example, colloidal dispersion has enabled the investigation of SWCNT optical properties, including absorbance and fluorescence.[3,8,9] The latter is being explored for many applications, including bioimaging in vitro[10] and in vivo[11,12] and single-molecule sensing.[13,14] Perhaps most importantly, colloidal dispersion has enabled SWCNT sorting by length and chirality, using techniques such as liquid chromatography,[15−17] ultracentrifugation,[18−20] field flow fractionation,[21] and selective precipitation.[22]

A basic requirement for working with colloidal SWCNTs is the determination of SWCNT carbon concentration, hereafter denoted as [C]. Perhaps the most accessible method is optical absorption-based concentration measurement.[23−25] However, the method has been a source of contention, because of the complicated nature of SWCNTs and differing basic assumptions used by different researchers. An optical absorption spectrum of colloidal SWCNTs can be described as having two main features: characteristic "peaks" corresponding to the one-dimensional excitonic transitions of the SWCNTs (E_{11}, E_{22}, ...), and a monotonically decaying "baseline" spanning from the UV region all the way to the near-IR region. If both features were intrinsic and invariant parts of the spectrum, [C] would be linearly proportional to the optical absorption at any wavelength. Indeed, recent results from particle tracking of fluorescent SWCNTs suggest this is the case for defect-free SWCNTs.[26] However in reality, it has been observed that the relative portion of the two features changes because of many intrinsic and extrinsic factors.[27] Perhaps most surprisingly, length-fractionated SWCNTs invariably show dramatically decreased peaks and increased baselines for shorter nanotubes,[19,22,23,28] despite otherwise having apparently the same extrinsic and intrinsic properties (e.g., chirality distribution, dispersion quality). It is evident, therefore, that for length-fractionated SWCNTs, the "peak" and "baseline" features are not invariant, and the use of absorption spectra to estimate concentration is not straightforward.

A simple quantification method is to use absorbance at the E_{11} peak as a proxy for [C]. This method would be most accurate if the baseline were a result of extrinsic factors, such as the presence of impurities,[23,27] and were subtracted from the spectrum entirely.[29] However, attributing the baseline to non-nanotube impurities appears to be problematic, because the baseline increase for short SWCNTs is observed in samples from both chromatography- and centrifugation-based fractio-

Received: July 17, 2012
Accepted: September 20, 2012
Published: September 20, 2012

   dx.doi.org/10.1021/ac302023n | *Anal. Chem.* 2012, 84, 8733−8739

nation techniques, and, therefore, the impurities must simultaneously match SWCNTs in such properties as density and hydrodynamic radius. Considering that no plausible impurity morphology seems to meet these criteria, Fagan et al. proposed that the baseline feature is an intrinsic part of the SWCNT spectrum, arising from the $\pi-\pi^*$ transition that should not vary with tube length.[28] Based on this line of argument, [C] can be most accurately measured by the baseline absorbance, i.e., at a wavelength with minimal contribution from excitonic transitions.[28] This approach was followed by Sun et al.[24] for calculating [C] of very short SWCNT samples. Thus, by assuming either the peak or baseline absorbance to be invariant with SWCNT length, different researchers have used either the peak or the baseline absorbance-based method to determine SWCNT carbon concentration.

Here, we establish the relationship between SWCNT carbon concentration, [C], and optical absorption spectra of colloidal SWCNT dispersions. The nanotubes are dispersed in water using a single-stranded DNA oligomer $(GT)_{20}$[30,31] and length-fractionated using a previously reported method: size-exclusion chromatography (SEC).[23] Since this process removes any unbound DNA, the concentration of remaining DNA may be used as a proxy for [C]. We confirm that the DNA:[C] mass ratio is constant for our length-fractionated samples by X-ray photoelectron spectroscopy (XPS). We then quantify the DNA in our samples using the fluorescent tag (Alexa Fluor 488),[32] which was integrated into the $(GT)_{20}$ oligomer during synthesis. We use the derived [C] to evaluate quantification methods based on the absorbance at the excitonic transition peak and at the baseline, as well as a new empirical method based on spectral integration of the E_{11} region, which we show is more accurate than previously proposed methods.[28] Finally, we examine some morphological features of colloidal SWCNTs, which may account for the widely observed spectral variations.

MATERIALS AND METHODS

Nanotube Dispersion. SWCNTs (grade S-P95-02-Dry, batch Du1-A001 CoMoCAT) were purchased from Southwest Nanotechnologies (Norman, OK).[32] A similar material is now available from Sigma–Aldrich as "Carbon Nanotube, single-walled, (6,5) chirality" (Catalog No. 704148). DNA oligomers, $(GT)_{20}$ and $(GT)_{20}$ labeled at the 5′ end with Alexa Fluor 488, were purchased from IDT-DNA (Coralville, IA). To make DNA-SWCNT, 40 mg of SWCNT powder were first suspended at a concentration of 1 mg/mL in deionized (DI) water by sonicating for 5 min with a 12.5-mm-diameter probe sonicator. This stock solution was used to create 4 mg pellets of SWCNT material in 1.5 mL centrifuge tubes for dispersion. To the 4 mg pellet were added 5 mg of $(GT)_{20}$ oligomer (10 mg/mL in DI water), DI water, and a buffer solution to the final concentration of 30 mmol/L sodium citrate, 300 mmol/L sodium chloride, pH 8. Nine percent (9%) of the oligonucleotides were labeled with Alexa Fluor 488 at the 5′ end. This mixture was sonicated, on ice, at 8 W with a 2-mm-diameter probe for 90 min. The resulting suspension was centrifuged at 18 °C and 17 000 g in 100 μL aliquots for 120 min. The supernatant was collected and combined for subsequent SEC fractionation.

SEC Fractionation. SEC was carried out as previously reported.[23] Briefly, silica-based SEC columns (Sepax CNT model) were purchased from Sepax Technologies, Inc. (Newark, DE), and used with a GE ÄKTA Purifier HPLC system. Three columns, with pore sizes of 2000, 1000, and 300 Å, respectively, and dimensions of 21.2 mm × 250 mm, were used in series. A total of 2 mL (8 mg of raw SWCNT material) of DNA-SWCNT dispersion were injected. The mobile phase consisted of 100 mmol/L NaSCN. This salt has been used for elution in the ion exchange separation of DNA-SWCNT.[5] We found, in this work, that NaSCN minimizes DNA-SWCNT binding to the SEC column, maximizing the yield. The flow rate was 4 mL/min, fractions of 5 mL were collected, and named sequentially from A1 to A15, followed by B1 to B15.

SWCNT Characterization. Optical measurements were carried out on a Varian Cary 5000 spectrophotometer and on a J-Y Horiba Nanolog 3 fluorimeter. Absorbance measurements were performed in a 10-mm-path-length microcuvette. For fluorescence measurements, samples were diluted to OD 0.02 at 488 nm and measured in a 2-mm excitation width/10-mm emission width/5-mm height microcuvette. Excitation at 488 nm was used and emission was collected in the 500–700 nm range. The measured fluorescence count was adjusted for dilution to reflect the original concentration of DNA-SWCNT in the sample. For surfactant displacement of DNA (see the Results section), sodium deoxycholate (SDC), 10% in DI water, was added to a final concentration of 0.4% and the sample was incubated for 2 h. No changes in fluorescence were observed with longer incubation.

For XPS, SEC samples were dialyzed against DI water for 4 days in a dialysis cassette (Novagen D-Tube Dialyzer Midi, MWCO 6–8 kDa, EMD Chemicals, Inc., San Diego, CA). Approximately 20 μL of this solution was dried on clean gold-sputtered silicon and rinsed with DI water to remove any residual soluble contaminants. XPS analysis was performed on a Kratos Axis Ultra spectrometer using monochromatized Al K_α radiation at 1486.6 eV. Survey spectra were taken at 90° (normal to the specimen surface) at multiple locations for each dried DNA-SWCNT specimen. Each survey spectrum was a sum of at least five scans acquired at pass energy of 160.0 eV and resolution of 0.5 eV/step. Dwell time was 100 ms/step for survey scans. A neutralizer gun was used to reduce charging of the samples. Binding energy corrections were made by referencing spectra to the C 1s peak at 285.0 eV. The program used for quantification was CasaXPS. The standard uncertainty associated with XPS measurement was 2%. Carbon contamination was subtracted from the samples by using clean gold substrate and sodium sulfate salt controls. This method gave the correct stoichiometric ratios (C:P and C:N) for $(GT)_{20}$ oligo controls.

Atomic force microscopy (AFM) imaging for rapid SWCNT length distribution measurement was carried out on a Bruker Dimension Icon system in peak-force tapping mode. Samples were prepared by diluting the SEC fractions by a factor of 20 with DI water and incubating for 20 min at room temperature on a silicon wafer substrate that was wiped clean with ethanol using a sheet of Kimwipe. For high-resolution AFM and impurity quantification, DNA-SWCNT were diluted by a factor of 10 into 15 mM KCl and deposited onto freshly cleaved mica by incubating for 5 min at room temperature and then rinsing with DI water. Imaging was then carried out on an Asylum MFP-3D AFM in tapping mode using an AC-160 model tip.

RESULTS AND DISCUSSION

SEC Fractionation. The elution profile for the SEC run, given by the absorbance at 780 and 990 nm (10-mm path length) is given in Figure 1A. Absorption spectra of three

dx.doi.org/10.1021/ac302023n | Anal. Chem. 2012, 84, 8733–8739

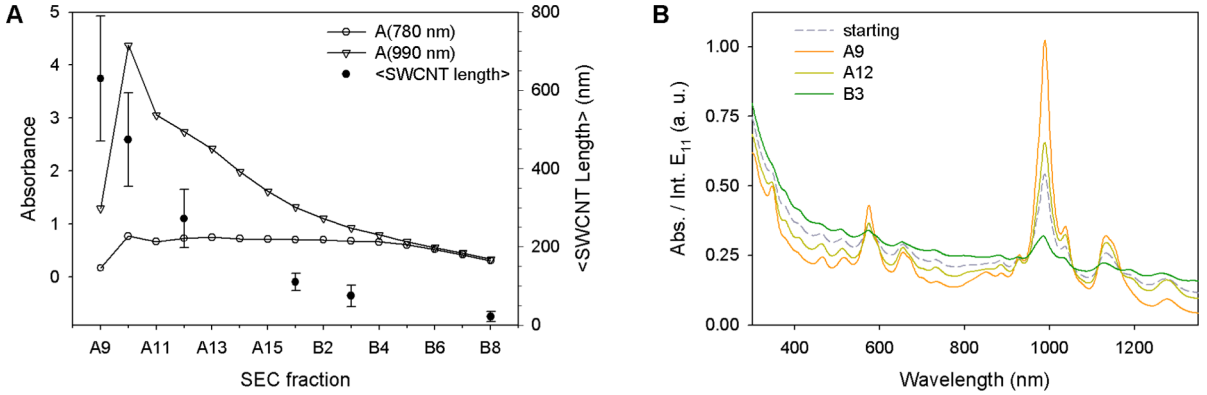

Figure 1. Length fractionation of DNA-SWCNT by SEC. (A) Elution profiles of the SEC run, along with mean fraction lengths. Error bars are ± one standard deviation in the length distribution. (B) The absorbance spectra of the starting material, as well as that of fractions A9, A12, and B3, normalized by spectral integration of the E_{11} region (780−1350 nm).

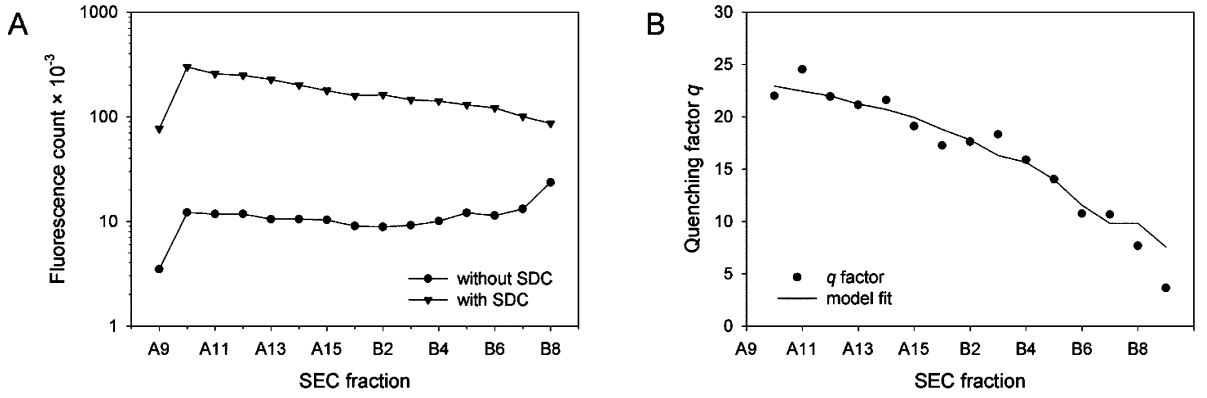

Figure 2. Fluorescence of Alexa Fluor-labeled DNA in the SEC fractions, before and after DNA stripping with SDC: (A) fluorescence count (518 nm emission/488 nm excitation) and (B) the fluorescence intensity ratio, termed the "quenching factor", and model fit.

selected fractions and the starting material are given in Figure 1B, normalized by the spectral integration of the E_{11} region (780−1350 nm). The spectra of the complete set of fractions are given in Figure S1 in the Supporting Information. Figure 1A also gives the average tube length of six selected fractions. As expected, shorter SWCNTs elute later. Histograms of the length distributions, as well as typical AFM images, are given in Figure S2 in the Supporting Information. These data are consistent with previously reported prep-scale SEC separations.[23]

For the CoMoCAT nanotube material used in this work, the absorbance from excitonic transitions reaches a local minimum at 780 nm, and we define this as "baseline" absorbance. Conversely, absorbance is highest at 990 nm, corresponding, for DNA dispersion, to the E_{11} transition of the abundant (6,5) tubes,[17] and we define this as "peak" absorbance. It is apparent from the elution profile that quantification based on peak absorbance A(990 nm), and the baseline absorbance A(780 nm), would give drastically different relative SWCNT carbon concentrations across the SEC fractions.

Determining SWCNT Carbon Concentration. SWCNTs are essentially one-dimensional (1D) objects, and the mass ratio of DNA to SWCNT is expected to be independent of SWCNT length. For single chirality samples, we previously confirmed this via capillary electrophoresis.[31] However, it has been proposed that SEC samples contain amorphous carbon impurities, which could alter the DNA:SWCNT mass ratio.[23] We measure this ratio via XPS survey spectra. To test the method, we measured the N:C and P:C ratio of pure $(GT)_{20}$ oligomer and obtained ratios of 0.39 ± 0.02 (0.36) and 0.09 ± 0.01 (0.10) (the expected stoichiometric molar ratios are given in parentheses). The ability to correctly determine the stoichiometric ratio of DNA implies that this method should give the correct DNA:SWCNT mass ratio. Using DNA as a calibration point, and averaging N:C and P:C data, we derived DNA:SWCNT mass ratios for A9, A13, and B3 to be 1.3 ± 0.1, 1.1 ± 0.1, and 1.3 ± 0.1, respectively.[33] Based on this result, we conclude that, within experimental error, the DNA:SWCNT mass ratio is independent of SWCNT length, and thus, as expected, DNA concentration may serve as a valid proxy for the nanotube mass concentration, at least in the length range considered here (630−70 nm).

We then measured the relative SWCNT carbon concentration in each SEC fraction by measuring the concentration of DNA. For DNA quantification, 9% of the $(GT)_{20}$ oligomers used in the dispersion were labeled with Alexa Fluor 488. Thus, the carbon concentration of SWCNTs is proportional to the fluorescence signal of the Alexa Fluor 488 dye. To exclude any influence on fluorescence from SWCNT, we stripped the DNA from the SWCNT surface with surfactant.

Fluorescence measurements on the fractions were carried out before and after the addition of SDC (see Figure 2A). As has been observed previously,[34,35] SWCNTs are strong fluorescence quenchers, and the DNA fluorescence signal is increased by as much as 20-fold by the addition of SDC. This is comparable to two values, 10-fold[34] and 17-fold,[35] reported for

dx.doi.org/10.1021/ac302023n | Anal. Chem. 2012, 84, 8733−8739

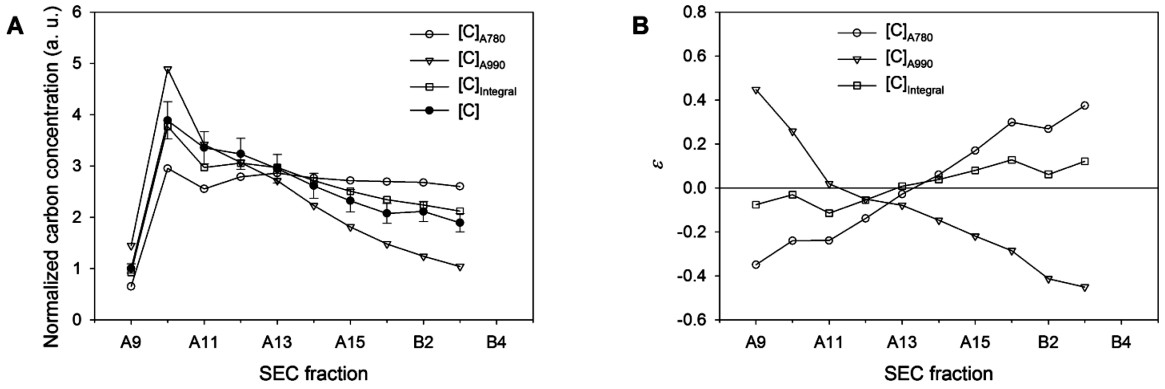

Figure 3. Comparison of SWCNT carbon concentration derived from the Alexa Fluor fluorescence intensity to concentrations derived from optical absorbance measurements. (A) SWCNT carbon concentration [C], compared to concentrations derived from absorbance values at 990 nm, ($[C]_{A990}$), 780 nm ($[C]_{A780}$), and the spectral integration from 780 nm to 1350 nm ($[C]_{Integral}$). [C] is normalized at the first fraction and the other traces are fit by a least-squares method. (B) Relative deviation of each absorbance-based method from [C].

fluorescein. Note that immediately after the SEC run, the surfactant-induced fluorescence change was smaller. The data reported here were taken after the samples were incubated for 5 days in order to achieve a stable level of fluorescence quenching by the SWCNT surface.

It is apparent from Figure 2 that the effective quenching factor (q), which is defined as the ratio of fluorescence intensity after DNA stripping to that before stripping, varies with the length of the SWCNT, being highest for the longest fractions. This can be explained by factoring in the behavior of DNA at the SWCNT end: since the Alexa Fluor 488 molecule is located at one end of the oligomer, there is some probability p that it will extend off the SWCNT and not be quenched. The effective quenching factor is then given by

$$q = \frac{(L/l)q_{CNT}}{(L/l) - p + pq_{CNT}} \quad (1)$$

where L is the length of the SWCNT, l the length of one $(GT)_{20}$ oligomer on the SWCNT, and q_{CNT} the quenching factor of Alexa Fluor 488 far from a SWCNT end. The length of a $(GT)_{20}$ on SWCNT is determined to be 9 nm, based on the DNA:SWCNT mass ratio measured by XPS, while L is obtained from AFM data shown in Figure 1A, interpolating for fractions not directly measured. The fit of eq 1 to the experimental data is shown in Figure 2B, yielding p = 0.2 and q_{CNT} = 24.

Testing SWCNT Quantification Methods. The XPS results indicate that the concentration of DNA in the sample is proportional to the SWCNT carbon concentration. Since we only obtained XPS data for fractions A9 (630 nm) to B3 (70 nm), we limit our analysis to tubes 70−630 nm in length. In this length range, the fluorescence count after DNA stripping with surfactant corresponds to the relative SWCNT carbon concentration, [C], in each sample (Figure 3A). The uncertainties shown by the error bars are calculated from the average uncertainty of the DNA:SWCNT ratios. We can now evaluate different carbon concentration measurements: based on baseline absorbance at 780 nm (A_{780}), on peak absorbance at 990 nm (A_{990}), and on the absorbance integral across the E_{11} region from 780 nm to 1350 nm ($A_{Integral}$). For each method, SWCNT carbon concentration is related to the absorbance value by a proportionality constant, which can be determined by least-squares fitting to [C] across SEC fractions. To evaluate quality of fitting, we define a merit function R^2:

$$R^2 = 1 - \frac{\sum_i ([C]_{i,X} - [C]_i)^2}{\sum_i (\overline{[C]} - [C]_i)^2} \quad (2)$$

where i is the fraction number, $\overline{[C]}$ is the mean carbon concentration, and X = "A780", "A990", or "Integral". The least-squares fits of $[C]_{A780}$, $[C]_{A990}$, and $[C]_{Integral}$ to [C] are plotted in Figure 3A. The uncertainties of absorption-based methods are estimated to be <0.1%. R^2 for these fits is 0.57, 0.53, and 0.95, respectively. Apparently, neither the peak absorbance nor the baseline absorbance can serve as a good proxy for the SWCNT carbon concentration. The integration method, which effectively averages the peak and baseline absorbance, comes closest to predicting the SWCNT carbon concentration. Integration over other regions, for example, from E_{33} to E_{11} transitions (300−1350 nm), gives similar results.

To further analyze the three quantification methods, we plot, in Figure 3B, the relative deviation ε of each absorbance-based measurement from [C], defined for each fraction i and each method X as

$$\varepsilon_{i,X} = \frac{[C]_{i,X} - [C]_i}{[C]_i} \quad (3)$$

As shown in Figure 3B, $[C]_{A780}$ diverges from [C], with $\varepsilon < 0$ for long SWCNTs and $\varepsilon > 0$ for short SWCNTs. We also tested concentration determination method using baseline absorbance at longer wavelengths, as has been reported,[28] and found that ε becomes even larger in these cases. $[C]_{A990}$ also diverges from [C]. In some reports, a fitted baseline was subtracted from the spectrum before E_{11} peak was used for the concentration measurement.[29] We tested this on our data and found that ε becomes larger. Overall, the integration method gives the smallest deviation.

The integration method could be used to determine the absolute concentration of similar SWCNT materials, using an integral extinction coefficient based on literature values. An extinction coefficient of (1100 ± 90) M^{-1} cm^{-1} at 990 nm peak absorbance has been reported for a CoMoCAT sample similar to the one used here.[36] Converting to the E_{11} integral basis, we obtain (2.5 ± 0.2) × 10^5 M^{-1} cm^{-1} nm. An extinction coefficient has also been reported for a single-chirality (6,5) SWCNT sample[25] (4400 ± 1000 M^{-1} cm^{-1}), which is (2.7 ± 0.6) × 10^5 M^{-1} cm^{-1} nm, in terms of the E_{11} integral.[33] The conversion to integral was performed by measuring samples similar to those used in the reports. These integral extinction

dx.doi.org/10.1021/ac302023n | Anal. Chem. 2012, 84, 8733−8739

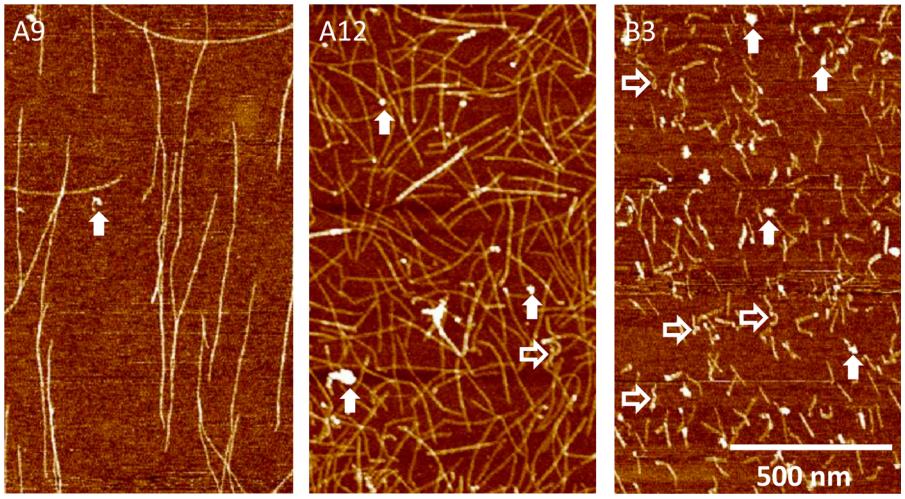

Figure 4. AFM images of three SEC fractions: A9, A12, and B3. The short nanotube fraction contains many curved SWCNTs (noted by open arrows) and many non-SWCNT impurities (noted by solid arrows). The longer fractions show straighter SWCNTs and fewer impurities.

coefficients may be used to estimate carbon concentrations for similar SWCNT materials.

Morphological Differences between Long and Short SWCNTs. Our observations imply that shorter SWCNT fractions have both higher baseline absorbance, and lower E_{11} transition peaks than longer fractions of the same concentration. The most likely cause, we speculate, is that the quality of short SWCNTs is inherently lower than of long SWCNTs. This idea was previously suggested by Cherukuri et al.[26] To test this, we examine morphological differences among different length fractions. We compare an AFM micrograph of fraction B3 to two longer fractions in Figure 4. Fraction B3 contains two types of objects which are sparse in A12 and nearly absent in A9: small objects much taller than the nanotubes (>2 nm, indicated by solid arrows), which we term non-nanotube impurities, and kinked or curved nanotubes (indicated by empty arrows), which we call defective SWCNTs.

Non-nanotube impurities are defined here as objects >2 nm in height, since all SWCNTs in the material examined here are <2 nm in diameter. For fraction B3, 18% of all observed objects were impurities, with an average height of 4 nm. In addition, 97% of all observed impurities were colocalized with SWCNTs. We speculate that these objects are graphitic catalyst cages or amorphous carbon left over from nanotube synthesis and covalently attached to the SWCNTs. This would explain why they are not sorted into shorter fractions during the SEC process. Assuming a spherical shape and the density of graphite, they correspond to 3% of the total carbon present in B3. The measured molar extinction coefficient of a close relative, carbon black, varies with preparation method, but is on the order of 500−1000 M^{-1} cm^{-1} at 780 nm.[27,37] The extinction coefficient for pure (6,5) SWCNTs is similar, ∼500 M^{-1} cm^{-1} at 780 nm.[25] Thus, the 3% carbon black-like impurities could only explain a small part of the observed increase in baseline absorbance.

SWCNT defectiveness may manifest itself in curved or tortuous nanotubes. It is evident from Figures 4 and 5 that short fractions contain kinked, curled, or otherwise tortuous SWCNTs, which have similar height as straight tubes. Examining fraction B3, we find that only 22% of SWCNTs are essentially straight, 25% are curved along their entire length, and the rest contain some kinked or curved segments. Curved

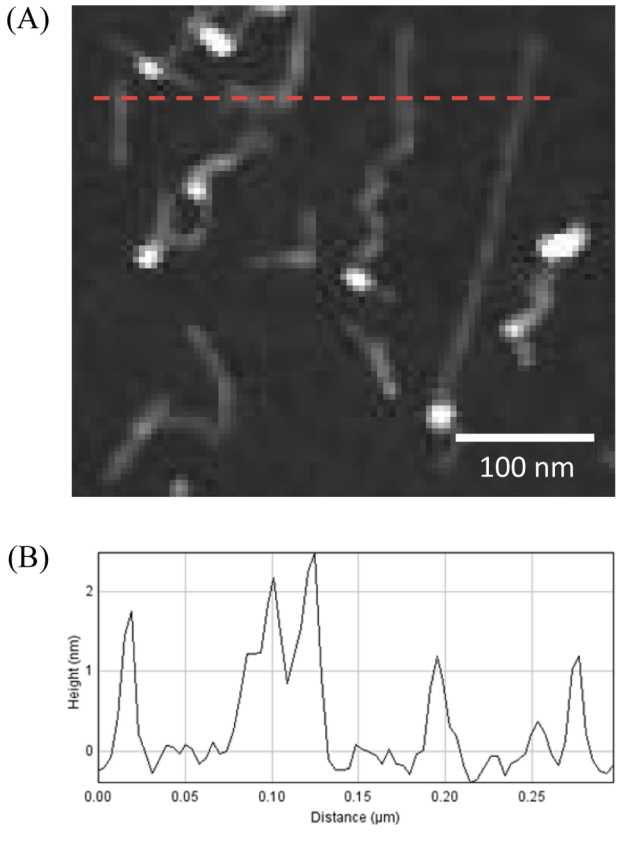

Figure 5. High-resolution image of straight and curved SWCNTs in fraction B3: (A) AFM micrograph and (B) height profile along the red dotted line.

DNA-SWCNTs have the same height as straight DNA-SWCNTs (see Figure 5) and fraction B3 has the same DNA:SWCNT ratio as fraction A9, which consists mainly of straight tubes; thus, defective tubes likely have similar DNA coverage. We propose that shorter nanotubes are more likely to be curved as a result of a greater defect density. Such defective nanotubes may break more easily during sonication, or grow to a shorter length during synthesis. We further propose that these defective nanotubes account for the higher baselines and lower excitonic transition peaks of the sample. Indeed, theoretical

dx.doi.org/10.1021/ac302023n | *Anal. Chem.* 2012, 84, 8733−8739

studies have shown that defects in nanotubes produce a simultaneous increase in baseline and diminution of the excitonic peaks.[38,39] These results are consistent with reported Raman measurements on length-sorted nanotubes, which have shown higher D/G′ ratios (the ratio of the Raman D band intensity to the G′ band intensity; this is a commonly used measure for defect concentration) for shorter SWCNT fractions.[40]

Length-dependent optical spectra have been observed for a variety of materials, including HiPCO, electric arc, and laser ablation materials.[19,28] We expect that, as SWCNT synthesis technology improves and the number of defective nanotubes is reduced, the effect that we observed may diminish or disappear altogether. For example, the new SG65i material available from Southwest Nanotechnologies (Norman, OK) shows less spectral change with length than the older SG65 material.

■ CONCLUSIONS

We have shown that simple colloidal single-wall carbon nanotube (SWCNT) carbon quantification methods based on excitonic peak absorbance or baseline absorbance are not accurate for length-fractionated samples. We have found that the integration of absorbance in the E_{11} region serves as a good concentration proxy for our samples. Based on literature values of SWCNT extinction coefficients, we have derived an integral extinction coefficient that may be used to calculate the carbon concentration of length-fractionated SWCNTs for similar materials. Furthermore, we have found that there are more curved tubes in shorter SWCNT fractions, likely due to greater defect density. This may explain why shorter SWCNT fractions have both lower excitonic transition peaks and higher baselines, and this may account for the failure of simple absorbance-based quantification methods. A logical extension of our conclusion is that straight, defect-free SWCNTs should have absorption spectra independent of tube length. Removing defective nanotubes to obtain samples with no spectral dependence on length will be the subject of a subsequent study.

■ ASSOCIATED CONTENT

Supporting Information

Complete UV−vis NIR absorbance spectra for the SEC separated fractions, as well as AFM length histograms and several AFM images. Additional details concerning XPS experiments are also given. This material is available free of charge via the Internet at http://pubs.acs.org.

■ AUTHOR INFORMATION

Corresponding Author

*ming.zheng@nist.gov.

Notes

The authors declare no competing financial interest.

■ ACKNOWLEDGMENTS

The authors would like to thank Dr. Angela R. Hight Walker and Dr. Rachel M. Stephenson for support and valuable discussions.

■ REFERENCES

(1) Bandow, S.; Rao, A. M.; Williams, K. A.; Thess, A.; Smalley, R. E.; Eklund, P. C. *J. Phys. Chem. B* **1997**, *101*, 8839−8842.
(2) Bonard, J. M.; Stora, T.; Salvetat, J. P.; Maier, F.; Stöckli, T.; Duschl, C.; Forró, L.; de Heer, W. A.; Châtelain, A. *Adv. Mater.* **1997**, *9*, 827−831.
(3) O'Connell, M. J.; Bachilo, S. M.; Huffman, C. B.; Moore, V. C.; Strano, M. S.; Haroz, E. H.; Rialon, K. L.; Boul, P. J.; Noon, W. H.; Kittrell, C.; Ma, J.; Hauge, R. H.; Weisman, R. B.; Smalley, R. E. *Science* **2002**, *297*, 593−596.
(4) Islam, M. F.; Rojas, E.; Bergey, D. M.; Johnson, A. T.; Yodh, A. G. *Nano Lett.* **2003**, *3*, 269−273.
(5) Zheng, M.; Jagota, A.; Strano, M. S.; Santos, A. P.; Barone, P.; Chou, S. G.; Diner, B. A.; Dresselhaus, M. S.; Mclean, R. S.; Onoa, G. B. *Science* **2003**, *302*, 1545.
(6) Wenseleers, W.; Vlasov, I. I.; Goovaerts, E.; Obraztsova, E. D.; Lobach, A. S.; Bouwen, A. *Adv. Funct. Mater.* **2004**, *14*, 1105−1112.
(7) Haggenmueller, R.; Rahatekar, S. S.; Fagan, J. A.; Chun, J.; Becker, M. L.; Naik, R. R.; Krauss, T.; Carlson, L.; Kadla, J. F.; Trulove, P. C.; Fox, D. F.; DeLong, H. C.; Fang, Z.; Kelley, S. O.; Gilman, J. W. *Langmuir* **2008**, *24*, 5070−5078.
(8) Bachilo, S. M.; Strano, M. S.; Kittrell, C.; Hauge, R. H.; Smalley, R. E.; Weisman, R. B. *Science* **2002**, *298*, 2361−2366.
(9) Lebedkin, S.; Hennrich, F.; Skipa, T.; Kappes, M. M. *J. Phys. Chem. B* **2003**, *107*, 1949−1956.
(10) Cherukuri, P.; Bachilo, S. M.; Litovsky, S. H.; Weisman, R. B. *J. Am. Chem. Soc.* **2004**, *126*, 15638−15639.
(11) Leeuw, T. K.; Reith, R. M.; Simonette, R. A.; Harden, M. E.; Cherukuri, P.; Tsyboulski, D. A.; Beckingham, K. M.; Weisman, R. B. *Nano Lett.* **2007**, *7*, 2650−2654.
(12) Welsher, K.; Sherlock, S. P.; Dai, H. *Proc. Natl. Acad. Sci. U.S.A.* **2011**, *108*, 8943.
(13) Cognet, L.; Tsyboulski, D. A.; Rocha, J.-D. R.; Doyle, C. D.; Tour, J. M.; Weisman, R. B. *Science* **2007**, *316*, 1465−1468.
(14) Jin, H.; Heller, D. A.; Kalbacova, M.; Kim, J. H.; Zhang, J.; Boghossian, A. A.; Maheshri, N.; Strano, M. S. *Nat. Nanotechnol.* **2010**, *5*, 302−309.
(15) Duesberg, G. S.; Muster, J.; Krstic, V.; Burghard, M.; Roth, S. *Appl. Phys. A: Mater. Sci. Process.* **1998**, *67*, 117−119.
(16) Huang, X.; Mclean, R. S.; Zheng, M. *Anal. Chem.* **2005**, *77*, 6225−6228.
(17) Tu, X.; Manohar, S.; Jagota, A.; Zheng, M. *Nature* **2009**, *460*, 250−253.
(18) Arnold, M. S.; Green, A. A.; Hulvat, J. F.; Stupp, S. I.; Hersam, M. C. *Nat. Nanotechnol.* **2006**, *1*, 60−65.
(19) Fagan, J. A.; Becker, M. L.; Chun, J.; Hobbie, E. K. *Adv. Mater.* **2008**, *20*, 1609−1613.
(20) Ghosh, S.; Bachilo, S. M.; Weisman, R. B. *Nat. Nanotechnol.* **2010**, *5*, 443−450.
(21) Chen, B.; Selegue, J. *Anal. Chem.* **2002**, *74*, 4774−4780.
(22) Khripin, C. Y.; Arnold-Medabalimi, N.; Zheng, M. *ACS Nano* **2011**, *5*, 8258−8266.
(23) Huang, X.; Mclean, R. S.; Zheng, M. *Anal. Chem.* **2005**, *77*, 6225−6228.
(24) Sun, X.; Zaric, S.; Daranciang, D.; Welsher, K.; Lu, Y.; Li, X.; Dai, H. *J. Am. Chem. Soc.* **2008**, *130*, 6551−6555.
(25) Schöppler, F.; Mann, C.; Hain, T. C.; Neubauer, F.; Privitera, G.; Bonaccorso, F.; Chu, D.; Ferrari, A. C.; Hertel, T. *J. Phys. Chem. C* **2011**, *115*, 14682−14686.
(26) Cherukuri, T. K.; Tsyboulski, D. A.; Weisman, R. B. *ACS Nano* **2012**, *6*, 843−850.
(27) Naumov, A. V.; Ghosh, S.; Tsyboulski, D. A.; Bachilo, S. M.; Weisman, R. B. *ACS Nano* **2011**, *5*, 1639−1648.
(28) Fagan, J. A.; Simpson, J. R.; Bauer, B. J.; Lacerda, S. H. D. P.; Becker, M. L.; Chun, J.; Migler, K. B.; Walker, A. R. H.; Hobbie, E. K. *J. Am. Chem. Soc.* **2007**, *129*, 10607−10612.
(29) Fantini, C.; Cassimiro, J.; Peressinotto, V. S. T.; Plentz, F.; Souza Filho, A. G.; Furtado, C. A.; Santos, A. P. *Chem. Phys. Lett.* **2009**, *473*, 96−101.
(30) Tu, X.; Zheng, M. *Nano Res.* **2008**, *1*, 185−194.
(31) Khripin, C. Y.; Manohar, S.; Zheng, M.; Jagota, A. *J. Phys. Chem. C* **2009**, *113*, 13616−13621.

(32) Certain commercial equipment, instruments, or materials are identified in this paper in order to specify the experimental procedure adequately. Such identification is not intended to imply recommendation or endorsement by the National Institute of Standards and Technology, nor is it intended to imply that the materials or equipment identified are necessarily the best available for the purpose. Unless noted otherwise, all reagents were obtained from standard sources.
(33) Here ± denotes the 95 % confidence interval.
(34) Yang, R.; Tang, Z.; Yan, J.; Kang, H.; Kim, Y.; Zhu, Z.; Tan, W. *Anal. Chem.* **2008**, *80*, 7408−7413.
(35) Yang, R.; Jin, J.; Chen, Y.; Shao, N.; Kang, H.; Xiao, Z.; Tang, Z.; Wu, Y.; Zhu, Z.; Tan, W. *J. Am. Chem. Soc.* **2008**, *130*, 8351−8358.
(36) Zheng, M.; Diner, B. A. *J. Am. Chem. Soc.* **2004**, *126*, 15490−15494.
(37) Jäger, C.; Henning, T.; Schlögl, R.; Spillecke, O. *J. Non-Cryst. Solids* **1999**, *258*, 161−179.
(38) Zhang, C.; Cao, J. C.; Guo, X. G.; Liu, F. *Appl. Phys. Lett.* **2007**, *90*, 023106.
(39) Charlier, J. C.; Ebbesen, T. W.; Lambin, P. *Phys. Rev. B* **1996**, *53*, 11108.
(40) Simpson, J. R.; Fagan, J. A.; Becker, M. L.; Hobbie, E. K.; Hight Walker, A. R. *Carbon* **2009**, *47*, 3238−3241.